RATE DEPENDENT ADHESIVE MODELING OF DUCTILE ADHESIVE COMPOSITE JOINTS

Ghazaleh Eslami[a], A. Vahid Movahedi-Rad[b] and Thomas Keller[c]

a: Ph.D. candidate at Composite Construction Laboratory (CCLab), École Polytechnique Fédérale de Lausanne (EPFL), Switzerland – ghazaleh.eslami@epfl.ch
b: Guest researcher at Composite Construction Laboratory (CCLab), École Polytechnique Fédérale de Lausanne (EPFL), Switzerland
c: Full professor at Composite Construction Laboratory (CCLab), École Polytechnique Fédérale de Lausanne (EPFL), Switzerland

Abstract: *The mechanical behavior of flexible adhesives used in fiber-polymer composite joints under monotonic and cyclic loading is highly nonlinear and sensitive to displacement rate in particular. To simulate their rate-dependent mechanical behavior, a phenomenological model was developed consisting of a linear and a nonlinear Maxwell unit acting in parallel. The viscoelastic parameters were calibrated by the results obtained from experiments under tension monotonic and reversed cyclic loadings. The applicability of the derived model is presented by power-law relationships between 1) the monotonic viscoelastic parameters and the applied displacement rates, and 2) the cyclic viscoelastic parameters and the maximum cycle displacements. The relationships enabled the simulation of both the pre- and post-yield monotonic and cyclic response characteristics, such as stretching of molecular chains (strain hardening), and formation and accumulation of damage (softening).*

Keywords: Adhesive-composite joint; ductile adhesive; rate-dependent behavior; constitutive equation; cyclic response

1. Introduction

In a load-bearing structure composed of brittle members, such as composite laminates, pseudo-ductility can be obtained by using a pseudo-ductile adhesive in the joints [1]. Due to the relatively high stiffness of the laminates compared to the adhesive in pseudo-ductile joints, the joints' response to the applied displacement mainly depends on the behavior of the adhesive. The adhesives used for structural purposes are mostly thermoset polymers and exhibit viscoelastic behavior [2].

In thermoset polymers, viscoelastic behavior is a result of molecular chain movements, which are both strain rate- and temperature-dependent [3]. Different applied strain rates can result in different mechanical responses in the polymer, varying from brittle to pseudo-ductile, with different yield load and post-yield behavior [4]. The thermoset molecular chain structure consists of both primary bonds (in the chains and cross-links between the chains, mainly covalent bonds) and secondary bonds (van der Waals and hydrogen bonds), whose strength decreases as the distance between the chains increases. Under applied low strain rates, the coiled chains have sufficient time to uncoil. After the yield point, chains start to lose secondary bonds and subsequently become aligned or stretched [5]. The stiffness thus significantly decreases and the deformability significantly increases; stretching may result in a hardening behavior. On the other hand, under high strain rates, the chains do not have sufficient time to

 ©2022 1st Author et al. https://doi.org/ 10.5075/978-X-XXX-XXXXX-X published under CC BY-NC 4.0 license

rearrange and respond to the imposed displacement, and the molecular mobility of the chains is reduced. Consequently, the stiffness remains high and deformability low [6]. Broken primary and lost secondary bonds contribute to the initiation and propagation of damage and energy dissipation in viscoelastic polymers [7].

Comprehensive constitutive models are valuable assets for analysis and design purposes and a wide range of constitutive models has therefore been developed for viscoelastic materials. The simplest mechanical model for viscoelastic behavior consists of two elements, each representing a mechanical characteristic of the behavior: a spring and a dashpot (or damper). A linear spring is used for modeling the elastic behavior where the spring constant, S, is the modulus of elasticity. A linear viscous dashpot contains a fluid with a viscosity η is used to model the viscous behavior [8]. Spring and dashpot elements can be combined in a variety of configurations to produce a desired viscoelastic response. Maxwell and Kelvin are the most basic models that combine a Hookean spring with a Newtonian dashpot, in series and parallel, respectively [9]. The combination of a simple spring and a dashpot element has been long used for simulating the rate-dependent behavior of viscoelastic materials [10].

Bergström and Boyce performed a study on the large-strain time-dependent behavior of elastomeric materials [11]. They proposed that the mechanical behavior of elastomeric materials can be decomposed into an elastic and a time-dependent segment (viscous segment) and modeled with nonlinear springs and a dashpot. Liu et al. [12] found that the Bergström and Boyce model was unable to identify the damage accumulation in filled rubbers to capture their rupture under cyclic loading. To capture stress-softening, i.e. damage accumulation, Ayoub et al. [13] proposed a phenomenological model which comprised a nonlinear spring in parallel with a nonlinear Maxwell element. In their model, they identified the average length of the chains and the average number of chains per unit volume as the physical parameters and modified both by a variable damage parameter.

In this study, to allow for a representative simulation of the pseudo-ductile behavior of adhesively-bonded fiber-polymer composite joints under various applied displacement rates, a novel phenomenological model is developed for the viscoelastic behavior of pseudo-ductile adhesives. The phenomenological model consists of two parallel units: a Maxwell unit characterizing the linear viscoelastic behavior before the onset of adhesive chain stretching, and a modified Maxwell unit with a variable stiffness spring that characterizes the nonlinear viscoelastic behavior during the molecular chain stretching. Unlike in literature, a unique constitutive equation is proposed for modeling both the monotonic and reversed cyclic behavior of the pseudo-ductile adhesive. The model parameters were calibrated with the results of monotonic and reversed cyclic experiments, previously performed in [14].

2. General phenomenological model

Double-lap joint specimens consisting of fiber-polymer composite adherends and a ductile adhesive were subjected to a series of monotonic tension and reversed cyclic tension-compression experiments; details of the experimental work and its motivation can be found in [14]. The load-joint displacement responses of the adhesive joints under monotonic and reversed cyclic loading are summarized in Fig. 1. Since the laminate stiffness was significantly greater than the adhesive stiffness and the contribution of the laminates to the joint displacements was thus negligible [14], the measured joint displacements, shown in Figs. 1 were

 ©2022 1st Author et al. https://doi.org/ 10.5075/978-X-XXX-XXXXX-X published under CC BY-NC 4.0 license

directly used for modeling the viscoelastic behavior of the adhesive. Furthermore, the cyclic responses (Fig. 1 (b), (c), and (d)) between the two reversal points of each cycle [14], followed the same pattern as the monotonic responses (Fig. 1 (a)). Therefore, the derived phenomenological model for the monotonic responses was applicable to the cyclic responses.

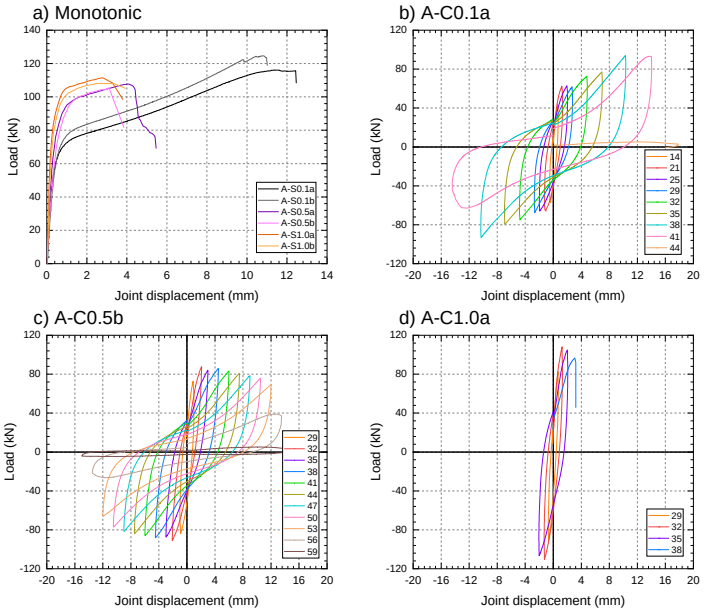

Figure 1. Load-joint displacement responses under a) monotonic loading under three displacement rates, and cyclic loading, primary cycles of b) A-C0.1a, c) A-C0.5b, d) A-C1.0a [14]

The investigated monotonic load-displacement curves were almost bilinear and thus consisted of two main branches, i.e., a pre-yield linear viscoelastic and a post-yield nonlinear viscoelastic branch, see Fig. 1 (a). Consequently, a phenomenological model composed of two dissimilar parallel Maxwell units was introduced, as shown in Fig. 2 (a). The first Maxwell unit includes a spring of constant stiffness and a dashpot in series, while the second unit consists of a spring with variable stiffness and a dashpot in series. The first Maxwell unit simulates the rate-dependent initial branch up to the yield point level as shown in Fig. 2 (b) (red line). The second Maxwell unit simulates the nonlinear stiffening due to the molecular chains' rate-dependent stretching up to the failure level, see blue line in Fig. 2 (b).

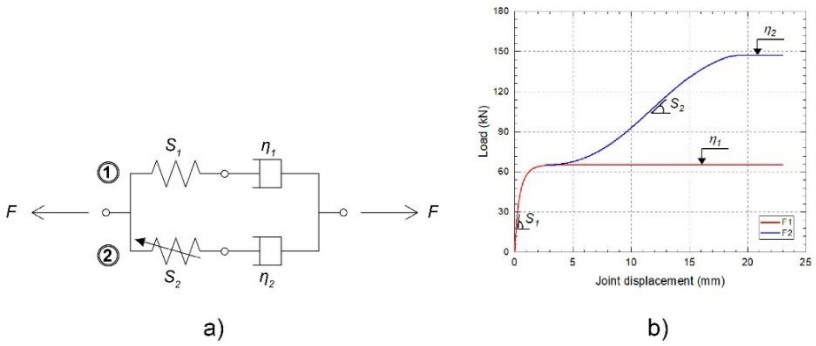

Figure 2. Rheological structure of phenomenological model

A mathematical model can be derived by combining the constitutive relationships of each Maxwell unit, considering force-displacement equilibrium and boundary conditions as follows:

 ©2022 1st Author et al. https://doi.org/ 10.5075/978-X-XXX-XXXXX-X published under CC BY-NC 4.0 license

$$X = X_1 = X_2 = \dot{X}t \quad (1)$$

$$F = F_1 + F_2 \quad (2)$$

where X is the total applied displacement, equal to the displacements of the first and second Maxwell units (X_1, X_2) in [mm], $\dot{X}$ is the applied displacement rate in [mm/s], and t is the time in [s]. Similarly, F is the total force, which is equal to the sum of the first and second Maxwell unit forces, F_1 and F_2, respectively, in [kN].

The force-displacement relationships in the Maxwell units can be expressed as follows [15]:

$$X_n = \left(\frac{1}{S_n} + \frac{1}{\eta_n \frac{\partial}{\partial t}}\right).F_n \ , \ n = 1,2 \quad (3)$$

where n is the number representing each of the Maxwell units. For the first Maxwell unit (n = 1), S_1 is the constant stiffness of the spring in [kN/mm], and η_1 is the viscosity coefficient of the dashpot in [kNs/mm]. For the second Maxwell unit (n = 2), S_2 is the variable stiffness of the spring to simulate the chain stretching effect on the load-displacement response, and η_2 is the viscosity coefficient of the second dashpot. Since the chain stretching causes a nonlinear increase in the adhesive stiffness, S_2 can be defined by a power-law relationship as follows [15]:

$$S_2 = \alpha \left(\frac{X}{\dot{X}}\right)^{\beta} \quad (4)$$

where α and β are fitting parameters defined for each cycle and displacement rate. By substituting the displacement equation (Eq. (1)) into the Maxwell unit relationships (Eq. (3) and (4)), the total load (Eq. (2)) can be calculated as follows:

$$F = \dot{X}\eta_1\left(1 - e^{-\lambda_1 t}\right) + \dot{X}\eta_2\left(1 - e^{-\frac{\lambda_2 t}{(\beta+1)}}\right) \quad (5)$$

where λ_1 and λ_2 are equal to S_1/η_1 and S_2/η_2, respectively. Parameters S_1, η_1, α, β, and η_2 are the considered viscoelastic parameters, to be determined for the development of the phenomenological model.

The optimization method used to estimate the viscoelastic parameters solved a nonlinear least-squares problem using the Trust Region Reflective (TRF) algorithm to apply error minimizing. The optimization task was performed using the Scipy.optimize library [16] in Python.

3. Monotonic and cyclic viscoelastic parameter results

3.1 Rate-dependent monotonic viscoelastic parameters

The load-displacement responses, obtained from the derived constitutive equation Eq. (5), are shown in Fig. 3 for the applied displacement rates of 0.1, 0.5, and 1.0 mm/s. The models agree well with the experimental results. The slight differences in the pre-yield linear segments of the phenomenological model and experimental curves were mainly due to the contribution of the laminate deformations, which became negligible after the yield points since the deformations in the adhesive increased significantly.

 ©2022 1st Author et al. https://doi.org/ 10.5075/978-X-XXX-XXXXX-X published under CC BY-NC 4.0 license

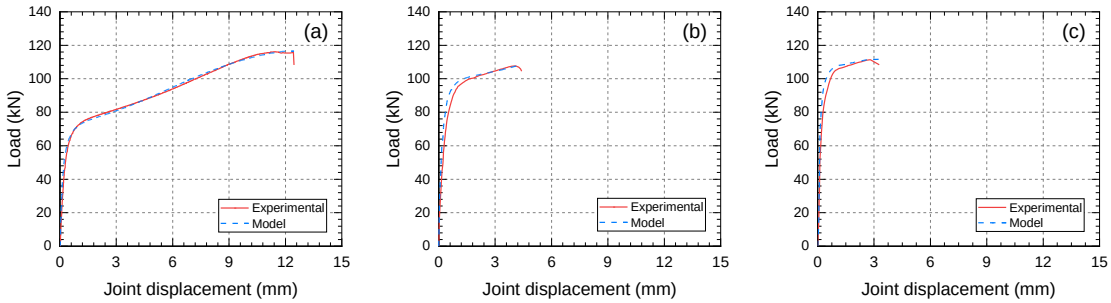

Figure 3. Phenomenological model and experimental load-displacement curves for displacement rates of: (a) 0.1 mm/s, (b) 0.5 mm/s, and (c) 1.0 mm/s.

The variations of the estimated viscoelastic parameters of the phenomenological model versus the applied displacement rates or joint displacement are shown in Fig. 4. The estimated values of S_1, η_1, and η_2, for the applied displacement rates of 0.1, 0.5, and 1.0 mm/s are shown with solid circles in Fig. 4 (a), (b), and (d) respectively, with added power-law fitted curves represented by dashed lines; the variable S_2 parameter is shown in Fig. 4 (c). By increasing the applied displacement rate, the S_1 parameter increased, while η_1, S_2, and η_2 decreased.

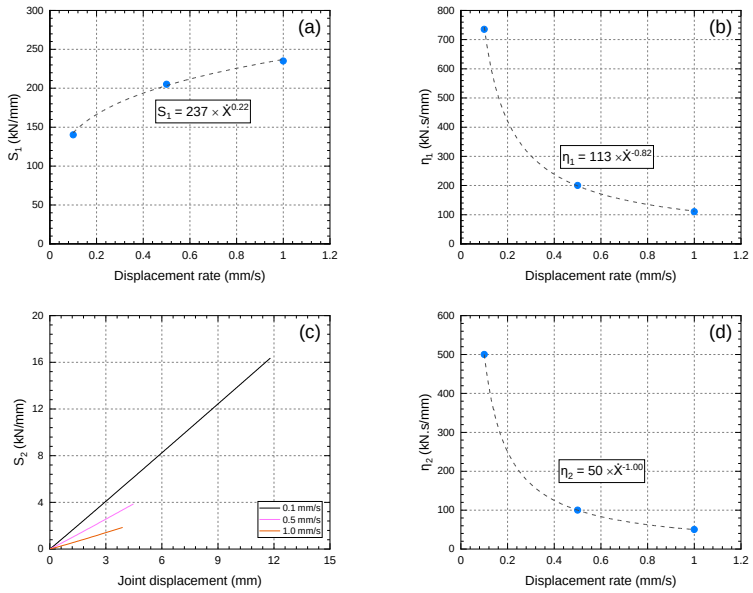

Figure 4. variation of monotonic viscoelastic parameters a) S_1, b) η_1, c) S_2, d) η_2.

3.2 Rate-dependent cyclic viscoelastic parameters

The cyclic responses of the specimens comprised primary and trailing cycles of which only the primary cycles are presented. Furthermore, by taking into account the different states of chains at the reversal points, each primary cycle response (Fig. 1 (b), (c), and (d)) was decomposed into T-P and P-P segments as 1) starting from the partially stretched state of the adhesive at the reversal point of the trailing cycle (T2) up to an almost fully stretched state at the first reversal point of the primary cycle (P1), and 2) starting from the latter (P1) to the also almost fully stretched state at the second reversal point of the primary cycle (P2) in the opposite direction.

The estimated viscoelastic parameters versus maximum cycle displacement (for S_1, η_1, and η_2) and cyclic displacement (for S_2), at each primary cycle, are shown in Fig. 5 for the applied

 ©2022 1st Author et al. https://doi.org/ 10.5075/978-X-XXX-XXXXX-X published under CC BY-NC 4.0 license

displacement rates, for partially and fully stretched states. The S_2 and η_2, parameters are not shown for the highest applied displacement rate of 1.0 mm/s due to the negligible amount of stretching.

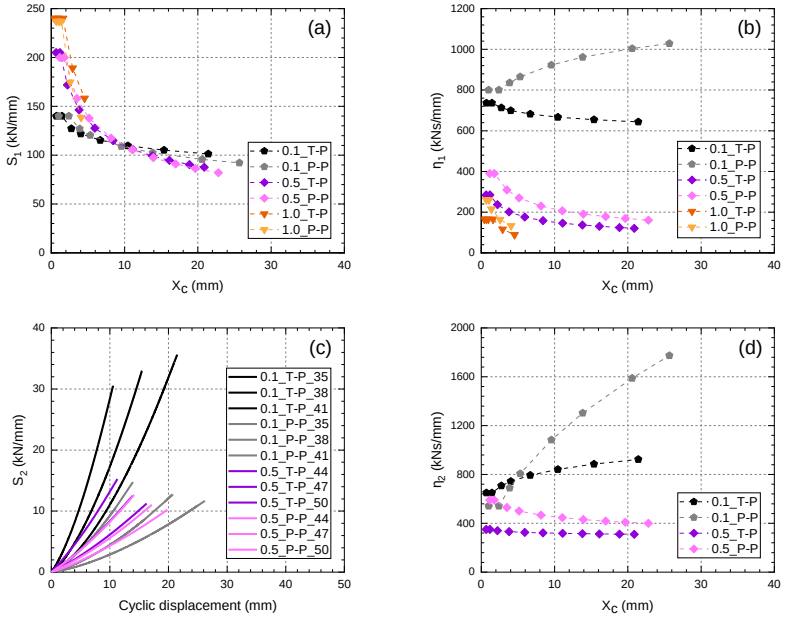

Figure 5. Variation of cyclic viscoelastic parameters, a) S_1, b) η_1, d) η_2, versus maximum cycle displacement, and c) S_2, versus cyclic displacement, under the applied displacement rates

The S_1 parameter values were initially higher at higher rates, see Fig. 5(a), but then decreased much faster than at the lower rate due to the higher loads (see Fig. 1), which increased damage formation and the associated softening. No significant differences could be observed for either of the states starting from partially or fully stretched materials.

The η_1 parameter values were higher at the lower rate and followed a decreasing trend with increasing applied maximum cycle displacements for all cases, except for the initially fully stretched material under the lowest 0.1 mm/s displacement rate, see Fig. 5(b). The accumulated damage generally decreased the viscosity parameters of the linear segment. In 0.1_P-P, however, the decreasing trend was reversed since the highly stretched chains at the reversal point first had to resist the reversed load until they ''buckled'', so to be realigned in the opposite direction.

The development of the S_2 parameter during each segment of the primary cycles is shown in Fig. 5(c). In all cases, the S_2 parameter exhibited an increasing trend due to an increasing number of aligned molecular chains with an increasing cyclic displacement. Under the lower applied displacement rate, due to the higher stretching in cycles with higher displacement, the maximum S_2 values increased in the T-P segments from each primary cycle to the next, while the slope of the curves decreased due to damage formation. In the P-P segments, the maximum S_2 values and slope of the curves (grey lines) were lower than in the T-P segments due to a delay in stretching. By increasing the cycle displacement, the delay in stretching in the opposite direction became more dominant and thus the S_2 maximum values decreased from each primary cycle to the next. At the higher applied displacement rate, much more damage was accumulated, which decreased both the S_2 maximum values and the slopes of the curves.

 ©2022 1st Author et al. https://doi.org/ 10.5075/978-X-XXX-XXXXX-X published under CC BY-NC 4.0 license

The η_2 parameter values were higher and increased for the lower 0.1 mm/s rate, and lower and decreased for the higher 0.5 mm/s rate (Fig. 5 (d)). The increasing-decreasing trends of the η_2 values were in line with the trends of the peak loads of each primary cycle (Fig. 1) since the former was determined from the latter (Fig. 2). The dominating hardening behavior at the lower rate increased the peak loads and thus η_2, while the dominating softening at the higher rate decreased the peak loads and η_2.

4. Model validation

The full cyclic responses of the experimental and phenomenological model under the displacement rate of 0.1 mm/s are compared in Fig. 6(a). The envelope curves of the experimental cyclic responses, shown in Fig. 1, and of the modeled cyclic responses, are further compared in Fig. 6(b). They were constructed by connecting the P1 peak loads. The comparison reveals that the hardening behavior under 0.1 mm/s and the softening behavior under 0.5 mm/s displacement rate were well represented in the model.

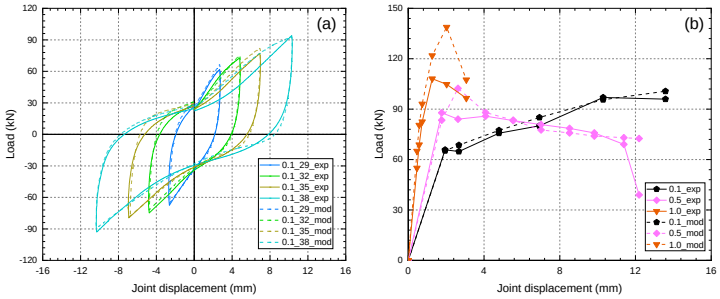

Figure 6. Experimental and modeled (a) load-displacement responses of full cycles for specimen A-C0.1a, and (b) envelope curves for specimen A-C0.1a and A-C0.5b at P1 reversal points

The comparison between the curves in Fig 6 validates the capacity of the phenomenological model to simulate the entire cyclic load-displacement behavior of the specimens.

5. Conclusions

A new phenomenological model was presented, allowing the simulation of the rate-dependent load-displacement responses of a pseudo-ductile adhesive joint under axial monotonic and cyclic loadings. By calibrating the viscoelastic parameters of the phenomenological model with the results from experimental monotonic and cyclic investigations, it could be concluded that:

1- The two Maxwell units of the phenomenological model were able to well simulate the rate-dependent pre- and post-yield branches of both monotonic and cyclic responses.

2- The viscoelastic parameters of the Maxwell units did capture well the physical characteristics of the adhesive in both monotonic and cyclic responses, such as stretching of molecular chains, and formation and accumulation of damage.

3- The effects of the applied displacement rate on the monotonic loading behavior were well represented by power-law relationships between the monotonic viscoelastic parameters and the applied displacement rates.

 ©2022 1st Author et al. https://doi.org/ 10.5075/978-X-XXX-XXXXX-X published under CC BY-NC 4.0 license

4- The proposed model could well predict the cyclic envelope curves, except for the final failure values of the last cycles. To also model the final chain scission, a third parallel unit could be added to the model, consisting of a dashpot element.

6. References

[1] Keller T, De Castro J. System ductility and redundancy of FRP beam structures with ductile adhesive joints. Compos Part B Eng 2005;36:586–96. https://doi.org/10.1016/j.compositesb.2005.05.001.

[2] Lancaster JF. The use of adhesives for making structural joints. Metall. Weld., Woodhead Publishing Series in Welding and Other Joining Technologies; 1999, p. 54–84. https://doi.org/10.1533/9781845694869.54.

[3] Ward IM, Sweeney J. Mechanical properties of solid polymers. vol. 1. 2013. https://doi.org/10.1016/0025-5416(67)90014-6.

[4] Angelidi M, Vassilopoulos AP, Keller T. Displacement rate and structural effects on Poisson ratio of a ductile structural adhesive in tension and compression. Int J Adhes Adhes 2017;78:13–22. https://doi.org/10.1016/j.ijadhadh.2017.06.008.

[5] Askeland DR, Wright WJ. The Science and Engineering of Materials. 7th Editio. Global Engineering: Timothy L. Anderson; 2014. https://doi.org/https://doi.org/10.1007/978-1-4899-2895-5.

[6] Foreman JP, Porter D, Behzadi S, Curtis PT, Jones FR. Predicting the thermomechanical properties of an epoxy resin blend as a function of temperature and strain rate. Compos Part A Appl Sci Manuf 2010;41:1072–6. https://doi.org/10.1016/j.compositesa.2009.10.015.

[7] Deblieck RAC, Van Beek DJM, Remerie K, Ward IM. Failure mechanisms in polyolefines: The role of crazing, shear yielding and the entanglement network. Polymer (Guildf) 2011;52:2979–90. https://doi.org/10.1016/j.polymer.2011.03.055.

[8] Brinson HF, Brinson LC. Polymer engineering science and viscoelasticity: An introduction, Second edition. 2015. https://doi.org/10.1007/978-1-4899-7485-3.

[9] Alfrey T, Doty P. The methods of specifying the properties of viscoelastic materials. J Appl Phys 1945;16:700–13. https://doi.org/10.1063/1.1707524.

[10] Schwarzl F, Staverman AJ. Time-temperature dependence of linear viscoelastic behavior. J Appl Phys 1952;23:838–43. https://doi.org/10.1063/1.1702316.

[11] Bergström JS, Boyce MC. Constitutive modeling of the time-dependent and cyclic loading of elastomers and application to soft biological tissues. Mech Mater 2001;33:523–30. https://doi.org/10.1016/S0167-6636(01)00070-9.

[12] Liu M, Hoo Fatt MS. A constitutive equation for filled rubber under cyclic loading. Int J Non Linear Mech 2011;46:446–56. https://doi.org/10.1016/j.ijnonlinmec.2010.11.006.

[13] Ayoub G, Zaïri F, Naït-Abdelaziz M, Gloaguen JM, Kridli G. A visco-hyperelastic damage model for cyclic stress-softening, hysteresis and permanent set in rubber using the network alteration theory. Int J Plast 2014;54:19–33. https://doi.org/10.1016/j.ijplas.2013.08.001.

[14] Eslami G, Yanes-Armas S, Keller T. Energy dissipation in adhesive and bolted pultruded GFRP double-lap joints under cyclic loading. Compos Struct 2020:112496. https://doi.org/10.1016/j.compstruct.2020.112496.

[15] Ferry JD. Viscoelastic properties of polymers. Third ed. John Wiley & Sons; 1980.

[16] Virtanen P, Gommers R, Oliphant TE, Haberland M, Reddy T, Cournapeau D, et al. {{SciPy} 1.0: Fundamental algorithms for scientific computing in Python}. Nat Methods 2020;17:261–72. https://doi.org/10.1038/s41592-019-0686-2.

 ©2022 1st Author et al. https://doi.org/ 10.5075/978-X-XXX-XXXXX-X published under CC BY-NC 4.0 license